https://doi.org/10.1016/j.ijrmhm.2021.105494

The material removal and the nanometric surface characteristics formation mechanism of TiC/Ni cermet in ultra-precision grinding

Yandan Zhu[1], Quanli Zhang[2*], Qingliang Zhao[3] and Suet To[4]

[1]Jiangsu Key Laboratory of Advanced Structural Materials and Application Technology, School of Materials Engineering, Nanjing Institute of Technology, Nanjing, 211167, China

[2]College of Mechanical and Electrical Engineering, Nanjing University of Aeronautics and Astronautics, Nanjing, 210016, China

[3]Centre for Precision Engineering, School of Mechatronics Engineering, Harbin Institute of Technology, Harbin, 150001, China

[4]State Key Laboratory of Ultra-precision Machining Technology, The Hong Kong Polytechnic University, Hong Kong

*Corresponding Author / E-mail: zhangql@nuaa.edu.cn, TEL: +86-25 84890644, FAX: +86-25 84891501

Abstract

In this paper, the material removal mechanism of TiC/Ni cermet is firstly investigated based on the analysis of the nano-indentation and the diamond scratching test, and the grinding induced surface damage mechanics is then explored according to the surface topography, the surface morphology and the material microstructure analysis. The results show that the material removal experienced plastic deformation, plowing and fracture under the dynamic scratching process, where the material microstructure plays a determinant role on the obtained surface characteristics of the TiC/Ni cermet. To achieve a smooth surface and ductile material removal by the ultra-precision grinding process, a group of the machining parameters is selected to reveal the formed nanometric surface characteristics, where the dislodgement of the hard TiC particles and the surface relief formation were induced by the varied material removal rate between the binding phases and the TiC hard particle under the scratching of the diamond grits. In addition, the preferred TiC (200) crystalline plane in the ground surface layer appears for the interface fracture between the TiC grains and the rim structure, while the Ni (111) crystalline plane shows a preferred growth for the extrusion in the subsurface deformed layer.

Keywords: TiC/Ni cermet; Mechanical loading; Surface damage; Nanometric surface characteristic

1. Introduction

Ti(C,N)/Ni cermet is now widely applied in the mechanical fields as the bearings and in the manufacturing area as the cutting tools due to the low friction coefficient, the superior high temperature hardness and the excellent chemical stability [1-5]. To further improve the toughness, the metal binder powders are usually added to the green body before the fabrication process, such as Ni and Co. However, a low toughness and strength resulting from the poor wetting of Ni on Ti(C,N) limits its wide application. Therefore, Mo element and WC grains are introduced to improve the wetting behavior by forming (Ti,Mo)(C,N) rim around the undissolved Ti(C,N) ceramic particles, as well as the refinement of the Ti(C,N) grains and strengthening the boundaries [4, 6-8]. After the sintering process, the microstructure of the obtained cermet is characterized by the hard cores surrounded by the multi rim layer, which greatly improves the toughness of the bulk materials by microcracking, bridging, cracking deflection, crack branching, etc [2].

However, the increased mechanical properties, as well as the non-uniformity of the material microstructure, make TiC based cermet quite difficult to be machined precisely with high surface integrity. The material removal behavior is dependent on the composite microstructure which greatly differs with the single-phase material. Taking the typical microstructure into consideration, the TiC core, the solid solution rim and the metal binder in TiC based cermet is obviously different from WC/Co cermet [9]. The indentation test and the diamond scratching process have been widely applied to investigate the material removal mechanism of hard and brittle materials [10-14]. The Vickers indentation, the nano-indentation and the diamond scratching results of the polished surface indicates that the ceramic-metal phase boundaries are easier to be broken for the formation of solid solutions during the fabrication of the TiC based cermets [15, 16]. The uneven grain size and the gradient microstructure result in the varying material removal mechanism and the more serious damage degree. For the improvement of the mechanical properties, the addition of the submicron TiC grains during the sintering process contributes to the obvious promotion of the mechanical properties and the obtained surface integrity after machining [3], which bears great

influence on the obtained tool life and the inaccurate form accuracy of product [5]. In addition, for the applications at high temperature, the micro-structural stability is also a key issue that should be evaluated during the machining process, where NiO, TiO_2, MnO_3 and Ti_2O_3 might be generated to form a loose layer that results in the increasing wear rate [4, 17]. Ultra-precision grinding process has been applied to machine the specific shape of the TiC based cermet [18, 19], where many micro-pits, surface reliefs and partial fracture of the TiC grains are identified on the ground surface except for the scratching grooves, and a subsurface damage layer of about 2.5 μm is induced [18], which is quite similar to the WC/Co hard metals under the same machining parameters [20]. Compared with the systematic and fundamental investigations on the cemented carbide of WC/Co, only a limited number of researches on TiC based cermets have been undertaken to reveal the machinability, the damage mechanics and the generated surface characteristics during the grinding process. On this basis, a comprehensive method, including the nanoindentation test, the Vickers indentation, the diamond scratching and the high spindle speed grinding, is employed in the present work to investigate the surface damage and the surface generation mechanism of TiC based cermet, combined with the necessary advanced surface characterization.

2. Materials and experiments

The studied TiC based cermet is mainly composed by the TiC and WC particles and the Ni, Co and Mo metal binders. The detail composition is listed in Table 1. Before the nano-indentation and the diamond scratching test, the workpiece surface was polished to achieve a surface roughness of $Sa < 15$ nm, as shown in Fig. 1.

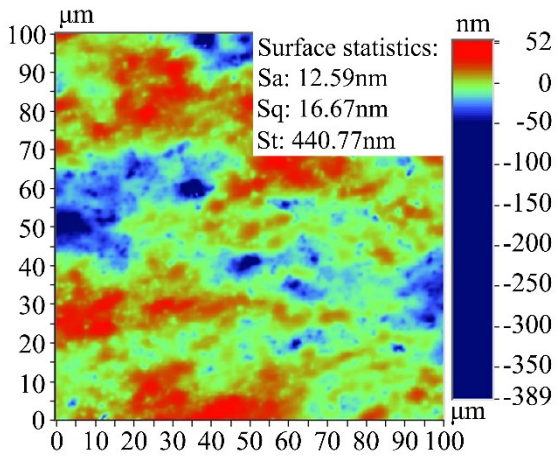

Fig. 1 Surface topography of the polished TiC/Ni cermet

The rotating diamond scratching test was undertaken on an ultra-precision surface grinding machine (MUGK7120X5, Hangzhou Machine Tool Group Co., Ltd, China), and the detail information of the test can be found in the previous study [21]. In addition, the nanoindentation test of the polished surface was performed on the Nano-indenter (NanoIndenter® XP system, MTS) under varying conditions with a Berkovich indenter. To investigate the material behavior under different loading speed, five repeated indentations at the maximum load of 100 mN by adjusting the loading/unloading time were undertaken.

The high spindle speed diamond wheel scratching was conducted on the machine tool of Moore Nanotech 450UPL, and the illustration of the grinding setup can be found in the previous work [22]. A resin bonded diamond wheel of 2000# was applied for the ultra-precision grinding of the TiC cermet after precision dressing by the green silicon stick and a diamond nib, where the detail grinding and dressing parameters are listed in Table 2.

Table 1 The detail composition of the workpiece material

Composition	TiC	WC	Ni	Mo	W	Others
Content (Vol.%)	60	15	13	4	3	5

Table 2 The detail grinding and dressing parameters

Grinding	$2000^{\#}$ diamond wheel	diam. 25 mm, resin bonded
	Concentration	75%

	Wheel RPM n_s (rpm)	50,000
	Workpiece RPM n_w (rpm)	120
	Feed rate f (mm/min)	0.5
	Depth of grinding a_e (μm/pass)	0.5
Truing	Truer	Silicon carbide stick/diamond nib
	Feed rate (mm/min)	0.5
	Depth of truing (μm/pass)	2
	Truer RPM (rpm)	200
	Wheel RPM (rpm)	3000
Coolant	CLAIRSOL 350	MQL

The surface morphology of the nano-indentation imprints was characterized by an optical microscope (OM, Olympus BX60) and a scanning electron microscope (SEM, Hitachi TM3000), and the surface morphology of the scratching grooves was also examined by the scanning electron microscope (SEM, Hitachi TM3000). The ground surface was then measured by another scanning electron microscope (SEM, JEOL Model JSM-6490), equipped with the energy dispersive X-ray spectroscopy (EDS). To characterize the nanoscale surface topography of the ground TiC based cermet, a white light interferometer (WLI, Nexview 3D profiler, ZygoLamda) and an atomic force microscope (AFM, Park's XE-70) were utilized. In addition, both Bragg Brentano X-ray diffraction (BBXRD, Rigaku SmartLab) and grazing incidence X ray diffraction (GIXRD, Rigaku SmartLab) were undertaken to analyze the phase structure of the original and the machined surface with the CuK_α radiation, where the incident angle for the GIXRD is 0.2°, 0.5°, 0.8° and 1.5°, respectively.

3. Results and discussion

To investigate the influence of the material microstructure, the nanoindentation test was conducted at varying positions at the maximum load of 100 mN under different loading/unloading time. The typical surface morphology of the imprints at the maximum load of 100 mN and the loading/unloading time of 20 s and 40 s is shown in Fig. 2, where the numbered imprints by green numerals are for the loading/unloading time of 40 s, and the pink numbers are labelled for the loading/unloading time of 20 s. It can be easily found that the material behavior under the nano-indentation test depends on the specific position where the composed phases differ at the selected positions. The different hardness for the composed phases, the different area ratio of the indents, and

the plastic deformation of the surrounding phases result in the inconsistent loading/unloading curves, as shown in Fig. 2(b) and Fig. 2(d). After a careful check of the surface morphology of the obtained indents, it is found that the typically obtained imprints can be classified into the pure indentation on TiC phase, the semi-mixed indentation on TiC phase and the rim structure, as well as the mixed indentation on TiC, the rim structure and the metal binder, as shown in Fig. 2(c). Specifically, the mixed modes of the indentation generally appeared for the random distribution of the TiC particles and the binder phases. To be mentioned, the pores in the bulk material bear obvious influence on the mechanic behavior under the nanoindentation test, where the singular loading/unloading curves for the numbered 3 and 4 positions by the green color appeared, as shown in Fig. 2(b). The lack of the support at the pore edge contributed to the fast deformation and uneven curves. In addition, it can be found that the indented imprints mainly experienced plastic deformation, and no obvious cracks are induced under the relative maximum load, even at the phase boundaries where the generated brittle phases by solid solution form [9].

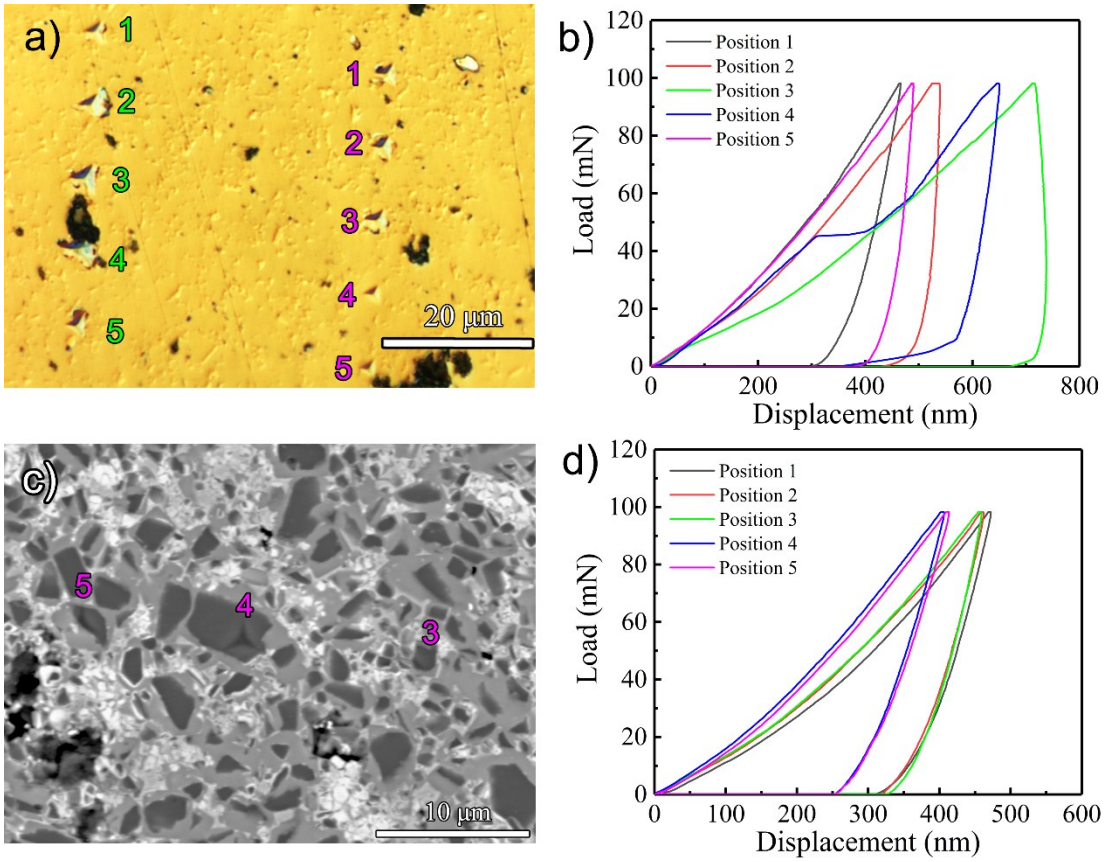

Fig. 2 Surface morphology of the nanoindents and the loading-displacement curves

for the nano-indentation test: (a) the surface morphology; (b) the loading-displacement curves at the maximum load of 100 mN for the loading/unloading time of 40 s (indicated by the green numbers); (c) SEM image of the typical imprints under different indentation mode at the maximum load of 100 mN for the loading/unloading time of 20 s (indicated by the pink numbers)

Actually, the material microstructure of the original TiC cermet has great influence on the obtained surface characteristic of the indented imprints. As shown in Fig. 3, the non-uniform distribution caused by the clustering of the TiC grains in the production process appears randomly. The lack of the binders in the clustering easily result in the formation of boundaries collapsion. Corresponding to the nano-indentaiton results, the loading-displacement curves is deformed as far as the indentation imprint involves the original defects in the bulk material.

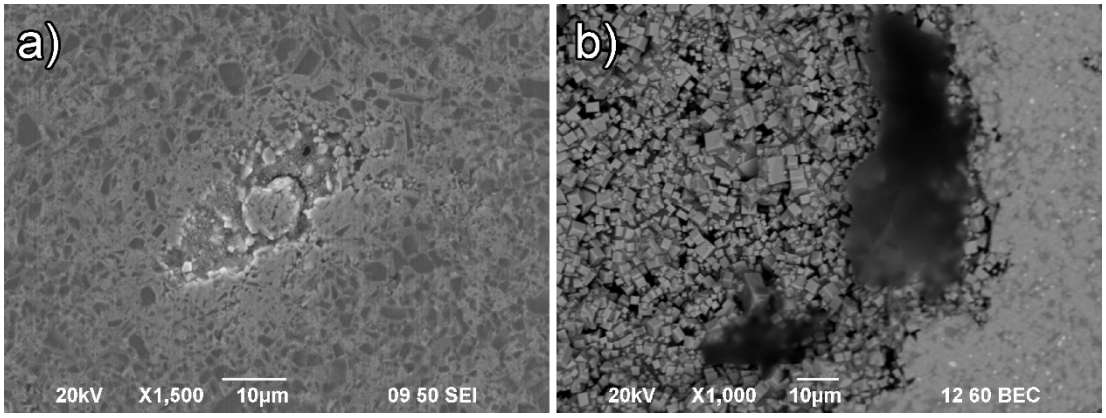

Fig. 3 Surface morphology of the micro-structure of the TiC based cermet

To get a further insight into the surface damage mechanism of the TiC-based cermet under the quasi-static loading condition, the Vickers indentation test under the load of 5 kg at varied points was undertaken. The surface morphology and the 3D surface topography of the indented imprints are shown in Fig. 4. The radial cracks formed at the four wedges of the diamond tips, and the cracks expanded twistedly. The intergranular cracks in the TiC grains mainly depend on the relative angle to the propogation tip. On the one hand, as the angle is greater than 30°, the transcrystalline cracks tends to be formed. On the other hand, the intergranular fracture is easier to be induced.

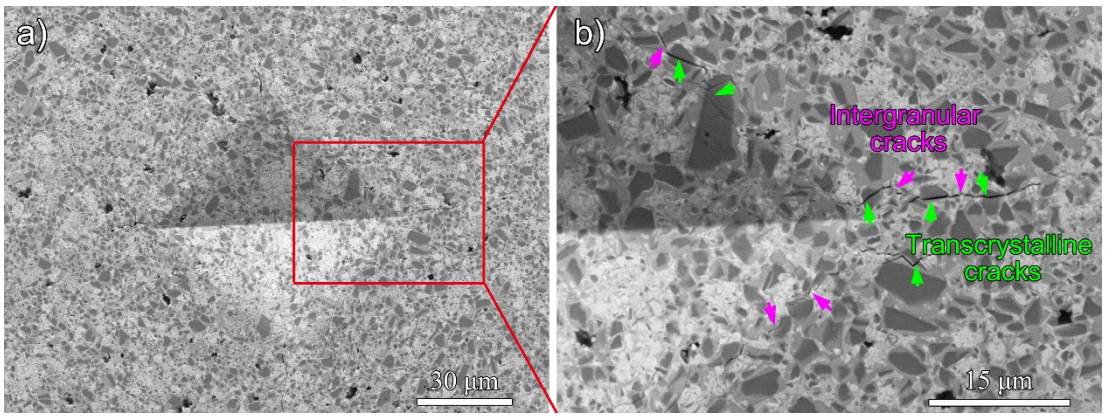

Fig. 4 SEM images of the Vickers indentation imprints of the TiC based cermet

The surface morphology of the diamond scratching grooves clearly shows that the material experienced three typical stages, as illustrated in Fig. 5(a), where the obvious plastic deformation under the moving diamond grit appeared at the first stage and no material removal was generated, as shown in Fig. 5(c). With increasing scratching depth, more serious deformation at the groove edge leads to the loose of the TiC particles under the squeezing effects of the diamond indenter, as shown in Fig. 5(b). The further growth of the scratching depth even resulted in the breakage of the surface to form the debris near the groove, which is marked by the pink arrows in Fig .5(b), Fig. (d) and Fig. 5(e). The micro tips on the diamond grits began to remove the material and the shape was copied to the bottom of the groove. Simultaneously, the material is removed with the hard particles and binders extruded under the diamond grits, as indicated by the red and the green arrows in the figures.

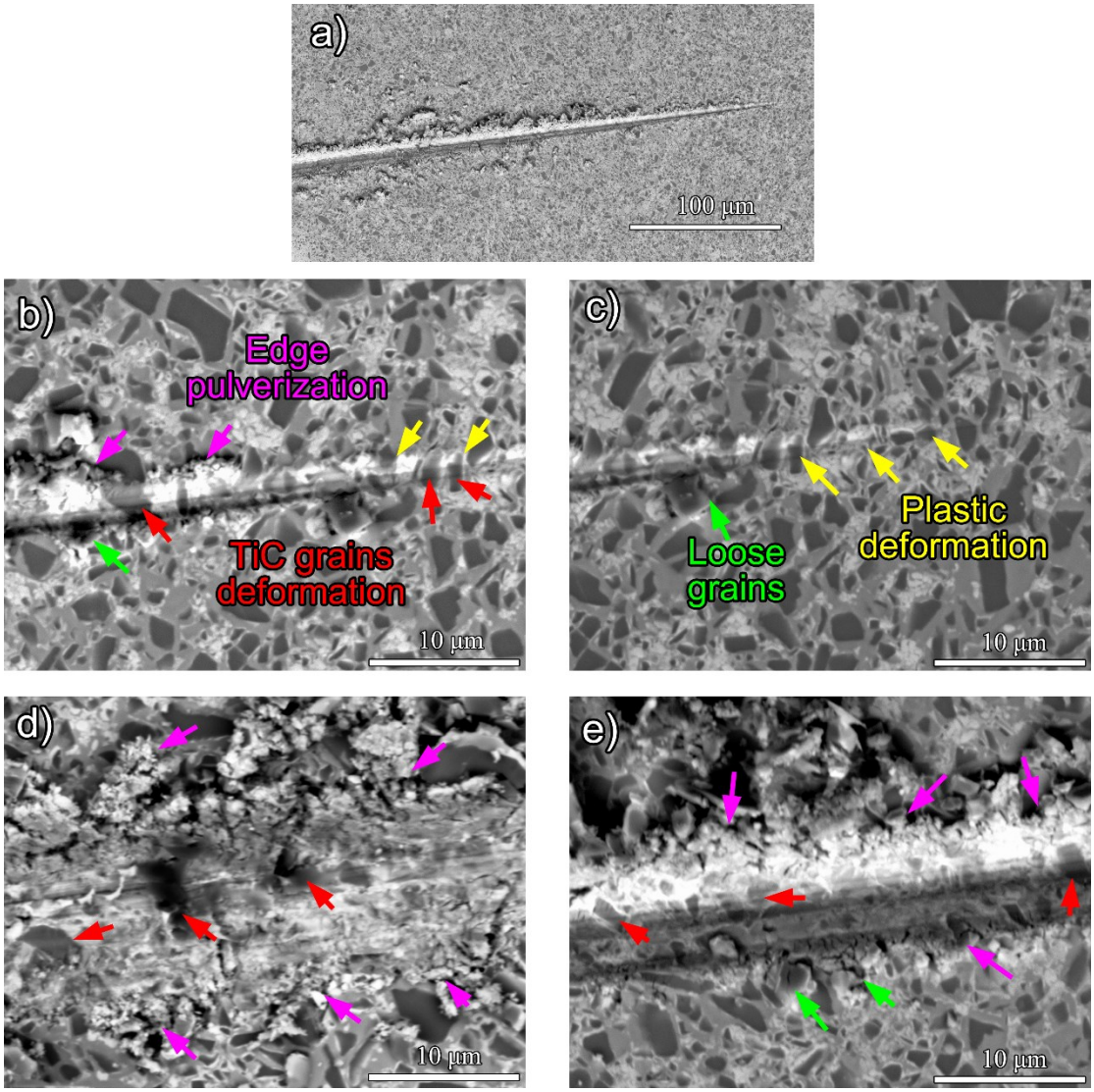

Fig. 5 Surface morphology of the diamond scratching grooves of the polished TiC based cermet

At the groove edge, the surface cracking is induced even after one time of scratching, which leads to the dislodgement of the particles in the multi-passes grinding process. To characterize the transition limit from plastic deformation to surface breakage and the surface cracking, the 3D surface topography and the cross-sectional profile along the scratching groove are collected by the white light interferometer (WLI), as shown in Fig. 6. The critical cutting depth from the plastic deformation to the appearance of the edge breakage is about 99.6 nm. Presumably, the porosity of the original material contributed to the plastic deformation at the initial stage. Even at the stage of the material removal, the actual cutting depth of the diamond grit drops compared with theoretical values based on the geometrical kinematics analysis.

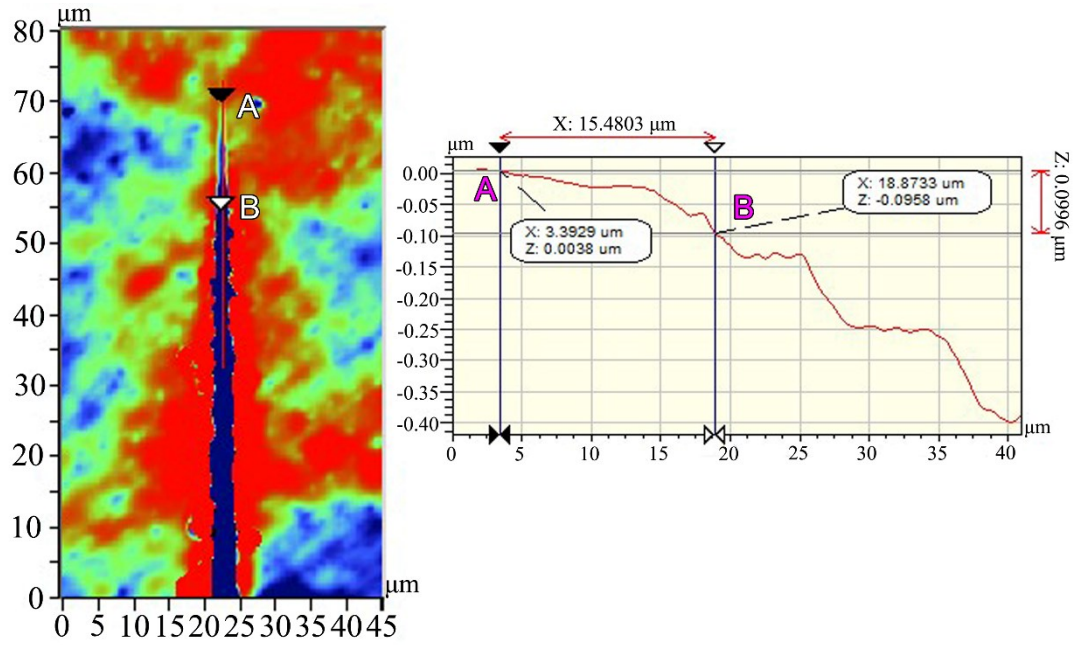

Fig. 6 Surface topography and the cross-sectional profile along the diamond scratching groove

Even though the diamond scratching results contributes to the understanding of the surface damage mechanism of the studied material, the low motion speed of the diamond tip always deviates from the actual machining speed, which results in the doubt of the reliability on the obtained achievements. Therefore, the high speed diamond scratching process and the high spindle speed diamond grinding process with a sharp V shape wheel are applied to explore the surface formation process [22, 23]. As shown in Fig. 7, the surface morphology of the diamond wheel grinding grooves indicates that the random protrusion height of the diamond grit in the wheel leads to the different material removal stage at the same grinding position for the diamond wheel. Specifically, the plastic deformation of the TiC based cermet was firstly induced under the normal pressure of the high spindle rotating wheel, where the material is not removed, as shown in Fig. 7(e). In addition, the edge of the pores in the original material experienced the early collapsion under the dynamic scratching of the sharp wheel before the grinding depth reaches the critical level, as indicated by the enlarged area in Fig. 7(d). The dislodgement of the TiC hard particles also results in the formation of the micro-pits in the grinding grooves, and the pulverization of the transition layer

composed of the brittle solid solutions was induced. Compared with the mechanical behavior of the WC/Co cemented under the same loading condition, it can be easily found that the TiC based cermet experienced an obvious plastic deformation stage before the material is removed [22], which resulted from the low density and the higher porosity of the bulk material.

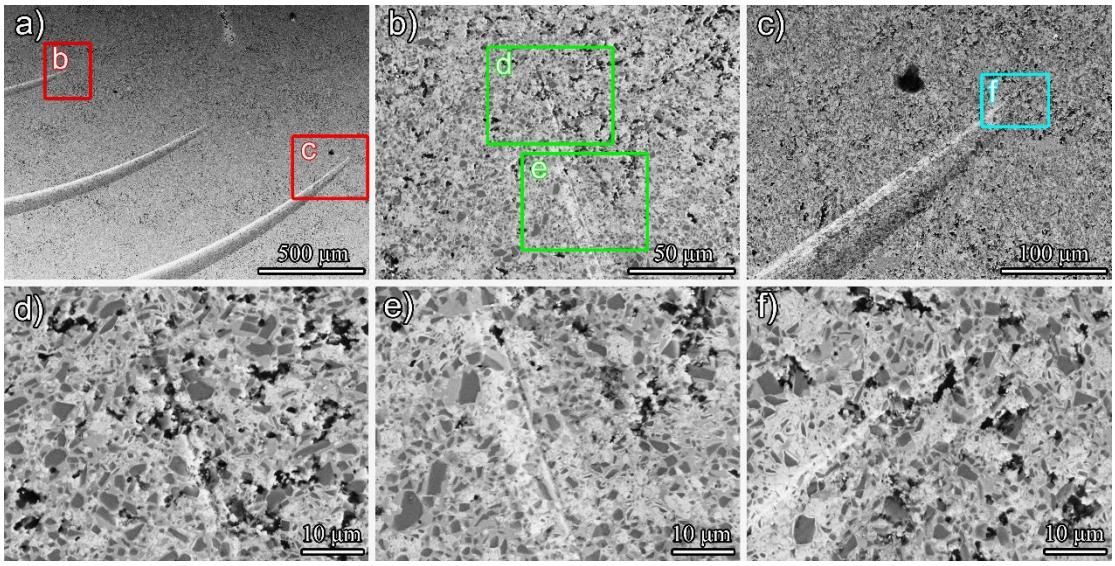

Fig. 7 SEM images of the high spindle speed diamond wheel scratching grooves of the TiC based cermet

Under the ultra-precision grinding process, the machined surface of the TiC based cermet is characterized by the scratching grooves, the grain fracture and the grain dislodgement, as shown in Fig. 8(a) and Fig. 8(b). It has been reported that the addition of the WC carbide grains decreases the wear resistance of the cermets due to the volatilization of tungsten oxide [24], and the wear mechanism of TiC based cermet was mainly micro-cracking induced spalling and abrasive wear, which turned to be adhesive and tribochemical wear [25]. The EDS results for the selected area A and B indicate that no serious oxidation was induced for both the TiC particles and the binder phase in the ultra-precision grinding process, as illustrated by Fig. 8(c) and Fig. 8(d). In addition, the phase boundaries between the hard TiC particles and the binders were always broken under the scratching of the diamond grits when the difference in the hardness resulted in the varying material removal rate between the binding phases and the hard particles, where less support for the edge area of the TiC particles occurs. Besides, the

repeated shock by the diamond grits also causes the fatigue of the binding interface. In combination with the generated micro-cracking, the dislodgement of the hard TiC particles can be easily induced.

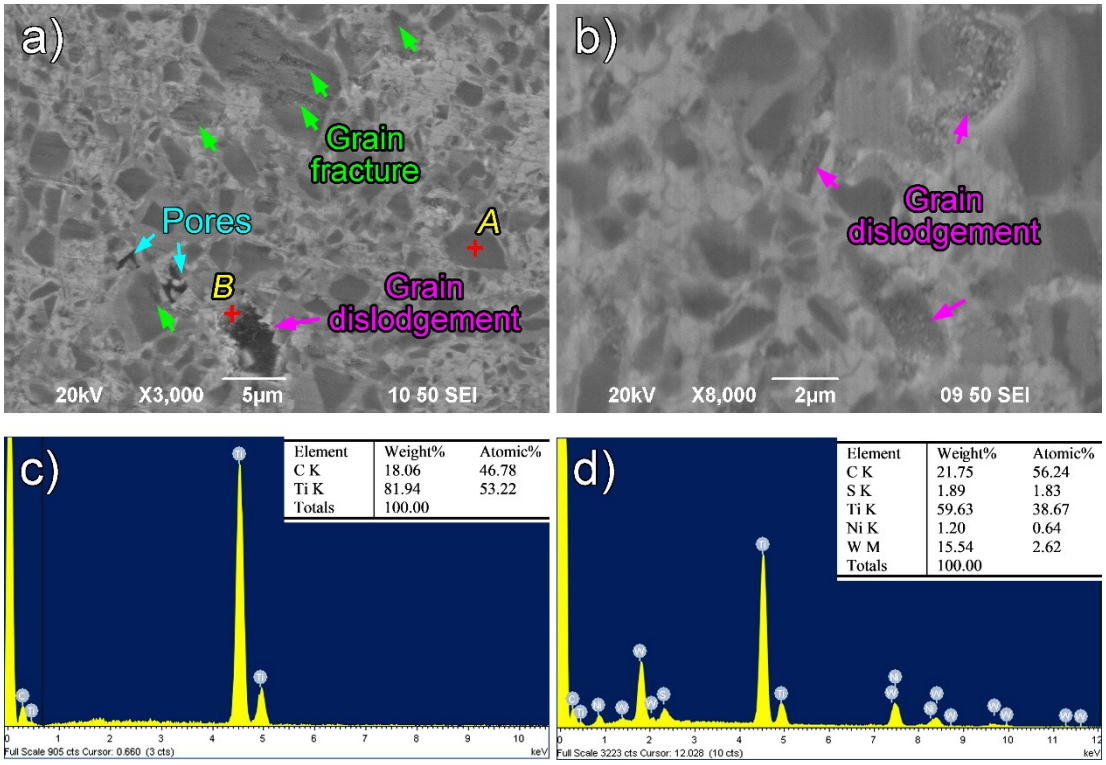

Fig. 8 Surface morphology of the TiC based cermet after ultra-precision grinding and the EDS results of the selected areas

The dislodgement of the TiC grains contributed to the formation of the micro-pits and the appearance of surface reliefs, as shown in Fig. 9(a). In addition, the related vibration between the grinding wheels and the workpiece also leaves some obvious marks on the machined surface. As illustrated in Fig. 9(b), the 2D FFT analysis of the obtained surface data shows that the main spatial frequency peaks correspond to the periodic marks induced by the tool feed and the tool vibration marks. Specifically, the peak at 236.5 1/mm is caused by the tool feed which is about 4.17 μm/r, and the peak at 37.1 1/mm is attributed to the relative vibration. In addition, the adjacent vibration and the phase shift also result in the appearance of some other spatial frequencies [26]. The weak peaks around the origin point should be induced by the randomly distributed micro-pits of various sizes, as shown in Fig. 9(c) and Fig. 9(d). In the feed marks, much finer scratching grooves occurred caused by the splintered diamond grit [27]. An

enlarged area of the formed micro-pits in Fig. 9(d) shows that the surface is covered by random fracture of the binding interface and the powder. The varying hardness of the composed phases contributed to the surface reliefs for the different material removal rate between the TiC and Ni phases.

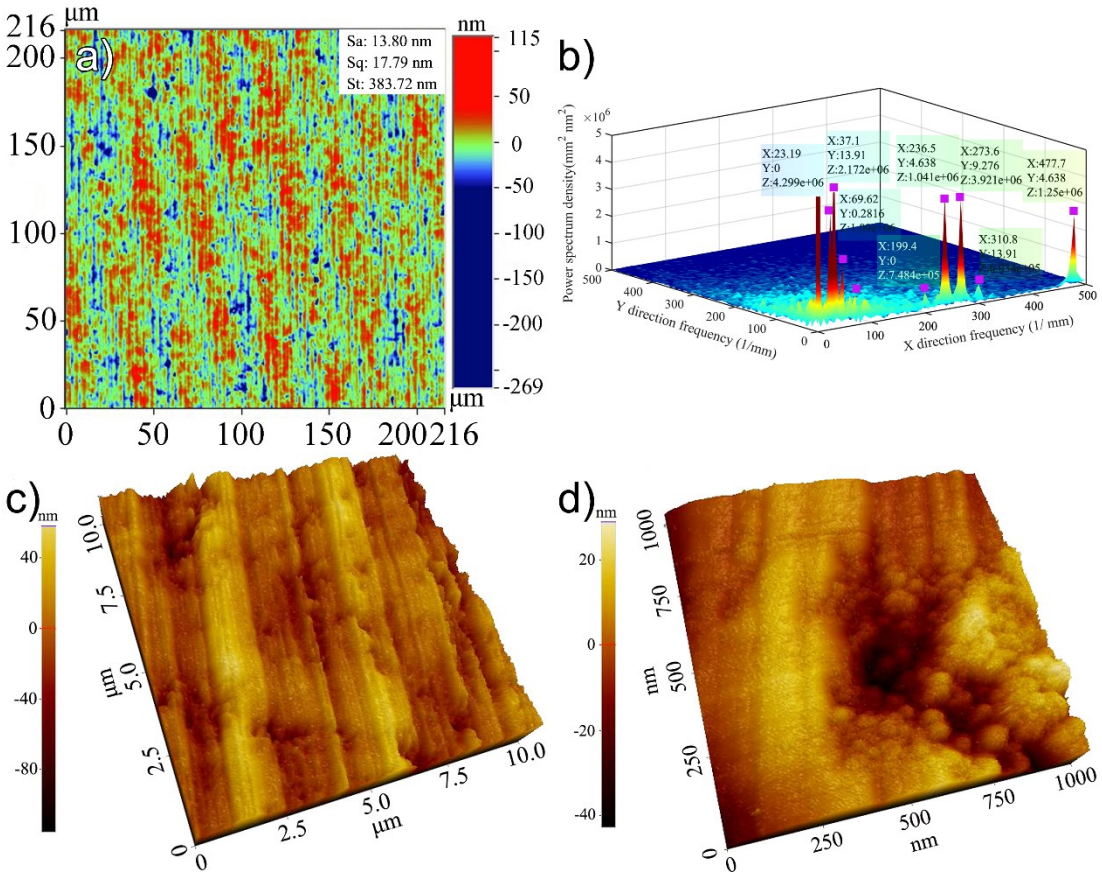

Fig. 9 3D surface topography and power spectra densities of the achieved 3D surface data by FFT: (a) 3D surface topography of the ground surface by the WLI, (b) FFT result of the obtained surface data, (c) and (d) the 3D surface topography by the AFM

The obtained BBXRD and GIXRD patterns of the ground surface are shown in Fig. 10. By comparing the typical peaks positions in the BBXRD patterns of the TN85 cermet before and after grinding, it can be easily found that the grinding process did not change the phase compositions of the TiC based cermet, which mainly contains TiC and Ni phases. The added WC, W and Mo are supposed to form (Ti, W, Mo)C solid solutions. Interestingly, the strongest peak intensity of the TiC phases changes from TiC(111) to be TiC(200), while the peak intensity for the Ni binders drops for the Ni (200) crystalline planes and the preferred crystalline planes growth of Ni (111) appears. The formation of the microcrystalline TiC grains induced by the surface fracture in the

grinding process should account for the increasing peak intensity for the TiC (200), and the extruded plastic deformation of the Ni binders and the preferred removal of Ni in the surface layer contribute to the dropped crystalline peaks. To get a further insight of the phase structure of the ground surface layer, the GIXRD results at different grazing incidence angle indicates that the peaks intensity for the detected TiC and Ni phases of the ground surface turns to be greater than the original material. Specifically, with the increasing incident angle from 0.2° to 1.5°, the peak intensity for TiC (111) gradually turns to be the strongest to be over TiC (200), which indicates the preferred grains orientation change in the ground surface. The fracture of the face centered TiC grains along the phase boundaries between the TiC (111) planes and the rim structure should account for the preferred crystalline plane in the ground surface. However, the peaks for Ni even does not occur for ground surface when the incident angle is below 0.5 °, indicating that the Ni binder in the outmost layer was removed in the grinding process. The further increase of the incident angle contributes to a higher penetration and characterizing depth. By comparing the results of the BBXRD and GIXRD, it can be derived that the extruded Ni binder in the subsurface layer along the grinding direction results in the preferred orientation of Ni (111), while the prior removal due to its low hardness leads to the peak disappearance in the outmost surface.

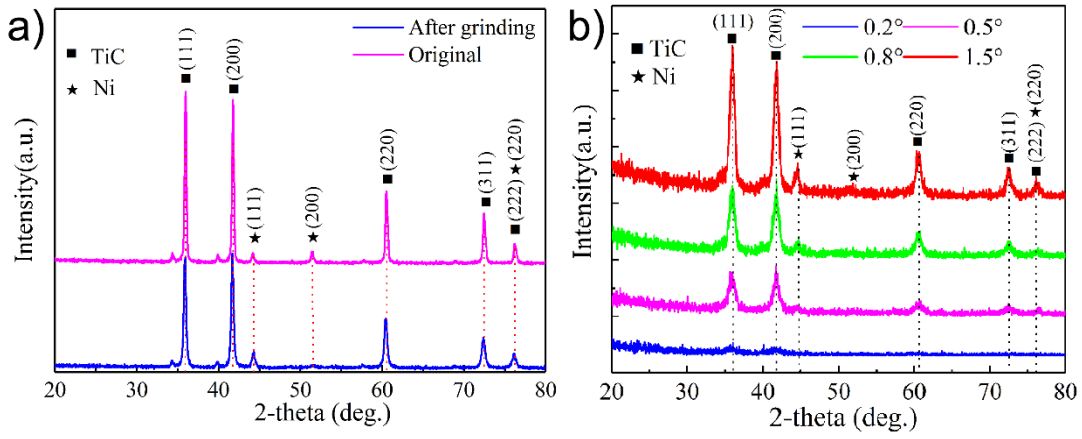

Fig. 10 BBXRD and GIXRD results of the machined TiC based cermet: a) BBXRD patterns, b) GIXRD patterns of the ground surface

4. Conclusions

This paper systematically investigates the surface generation mechanism,

including the typical surface morphology, the material removal mechanism and the surface damage modes, of the TiC based cermet under the quasi-static indentation, the dynamic diamond scratching and the high spindle speed grinding process. Combined with the various surface characterization results, the following conclusions are drawn:

(1) The surface damage mechanism of TiC based cermet mainly involves plastic deformation, brittle fracture of the gray rim, TiC grains fracture and dislodgements which results in the surface micro-pits formation on the machined surface after the ultra-precision grinding process;

(2) The material microstructure obviously affects the generated surface characteristics under the mechanical loading, where the uneven distribution of the composed phases and the porosity in the bulk material contributed to the easier fracture and pulverization of the edge area under the dynamic loading process;

(3) The difference in the mechanical of the hard particles, the gray rim and the binder phase leads to the varying material removal rate in the ultra-precision grinding process, and the ground surface is characterized by the plastic grooves and the micro-pits, where no evident oxidation is induced.;

(4) The grinding surface is characterized by the preferred TiC (200) crystalline planes caused by the interface fracture between the TiC phases and the rim structure, and the subsurface deformation results in the extrusion of the Ni binder, which contributes to the preferred Ni (111) plane orientation.

5. Acknowledgements

This work was supported by the National Natural Science Foundation of China (NSFC) (Project No.: 51805257), the Natural Science Foundation of Jiangsu Province (Project No.: BK20201298 and BK20201033), the China Postdoctoral Science Foundation funded project (Project No.: 2019TQ0151), and the University Research Foundation of Nanjing Institute of Technology (Project No. YKJ201805).

Declaration of Competing Interest

The authors declare that they have no known competing financial interests or personal relationships that could have appeared to influence the work reported in this paper.

6. References

[1] Q. You, J. Xiong, Z. Guo, J. Liu, T.E. Yang, C. Qin, Microstructure and properties of CVD coated on Ti(C,N)-based cermets with varying WC additions, International Journal of Refractory Metals and Hard Materials 81 (2019) 299-306.

[2] H. Liu, Y. Chai, C. Huang, H. Liu, J. Wang, Effect of boron nitride nanotubes content on mechanical properties and microstructure of Ti(C,N)-based cermets, Ceramics International 41 (2015) 2813-2818.

[3] A. Demoly, W. Lengauer, C. Veitsch, K. Rabitsch, Effect of submicron Ti(C,N) on the microstructure and the mechanical properties of Ti(C,N)-based cermets, International Journal of Refractory Metals and Hard Materials 29 (2011) 716-723.

[4] Q. Yang, W. Xiong, S. Li, Z. Yao, X. Chen, Early high temperature oxidation behaviour of Ti(C,N)-based cermets in air, Corrosion Science 52 (2010) 3205-3211.

[5] S.S. Sarjana, I. Bencheikh, M. Nouari, A. Ginting, Study on cutting performance of cermet tool in turning of hardened alloy steel, International Journal of Refractory Metals and Hard Materials 91 (2020) 105255.

[6] S. Chu, G. Liu, H. Xiong, Z. Li, K. Zhou, High-quality Ti(C,N)-based cermets via solid-state nitrogen-pressure sintering: Influence of the sintering atmosphere, International Journal of Refractory Metals and Hard Materials 92 (2020) 105291.

[7] W. Lengauer, F. Scagnetto, Ti(C,N)-based cermets: Critical review of achievements and recent developments, Solid State Phenomena 274 (2018) 53-100.

[8] C. Yi, H. Fan, J. Xiong, Z. Guo, G. Dong, W. Wan, H. Chen, Effect of WC content on the microstructures and corrosion behavior of Ti(C, N)-based cermets, Ceramics International 39 (2013) 503-509.

[9] N. Liu, S. Chao, X. Huang, Effects of TiC/TiN addition on the microstructure and mechanical properties of ultra-fine grade Ti(C,N)-Ni cermets, Journal of the European Ceramic Society 26 (2006) 3861-3870.

[10] J. Wang, B. Guo, Q. Zhao, C. Zhang, Q. Zhang, H. Chen, J. Sun, Dependence of material removal on crystal orientation of sapphire under cross scratching, Journal of the European Ceramic Society 37 (2017) 2465-2472.

[11] J. Wang, B. Guo, Q. Zhao, C. Zhang, Q. Zhang, W. Zhai, Evolution of material

removal modes of sapphire under varied scratching depths, Ceramics International 43 (2017) 10353-10360.

[12] C. Li, F. Zhang, X. Wang, X. Rao, Repeated nanoscratch and double nanoscratch tests of Lu2O3 transparent ceramics: Material removal and deformation mechanism, and theoretical model of penetration depth, Journal of the European Ceramic Society 38 (2018) 705-718.

[13] M. Gee, K. Mingard, J. Nunn, B. Roebuck, A. Gant, In situ scratch testing and abrasion simulation of WC/Co, International Journal of Refractory Metals and Hard Materials 62 (2017) 192-201.

[14] M. Bľanda, A. Duszová, T. Csanádi, P. Hvizdoš, F. Lofaj, J. Dusza, Indentation hardness and fatigue of the constituents of WC–Co composites, International Journal of Refractory Metals and Hard Materials 49 (2015) 178-183.

[15] M. de Nicolás, H. Besharatloo, J.M. Wheeler, M. de Dios, P. Alvaredo, J.J. Roa, B. Ferrari, L. Llanes, E. Gordo, Influence of the processing route on the properties of Ti(C,N)-Fe15Ni cermets, International Journal of Refractory Metals and Hard Materials 87 (2020) 105046.

[16] H. Zhou, C. Huang, B. Zou, H. Liu, H. Zhu, P. Yao, J. Wang, Effects of metal phases and carbides on the microstructure and mechanical properties of Ti(C,N)-based cermets cutting tool materials, Materials Science and Engineering: A 618 (2014) 462-470.

[17] L. Zhang, Y. Feng, Q. Nan, R. Ke, Q. Wan, Z. Wang, Effects of titanium-based raw materials on electrochemical behavior of Ti(C,N)-based cermets, International Journal of Refractory Metals and Hard Materials 48 (2015) 11-18.

[18] B. Guo, Q. Zhao, H. Li, Ultraprecision grinding of TiC-based cermet hemisphere couples, The International Journal of Advanced Manufacturing Technology 73 (2014) 1281-1289.

[19] Q. Zhang, Q. Zhao, S. To, B. Guo, A further study of wheel normal grinding of hemisphere couples on TiC-based cermet, The International Journal of Advanced Manufacturing Technology 87 (2016) 2593-2602.

[20] Q. Zhang, S. To, Q. Zhao, B. Guo, M. Wu, Effects of binder addition on the surface

generation mechanism of WC/Co during high spindle speed grinding (HSSG), International Journal of Refractory Metals and Hard Materials 59 (2016) 32-39.

[21] Q. Zhang, Q. Zhao, H. Su, S. To, A systematic investigation on the diamond wear mechanism during the dry scratching of WC/Co, International Journal of Refractory Metals and Hard Materials 70 (2018) 184-190.

[22] Q. Zhang, S. To, Q. Zhao, B. Guo, Surface generation mechanism of WC/Co and RB-SiC/Si composites under high spindle speed grinding (HSSG), International Journal of Refractory Metals and Hard Materials 56 (2016) 123-131.

[23] Z. Zhang, D. Guo, B. Wang, R. Kang, B. Zhang, A novel approach of high speed scratching on silicon wafers at nanoscale depths of cut, Scientific Reports 5 (2015) 16395.

[24] Y. Peng, H. Miao, Z. Peng, Development of TiCN-based cermets: Mechanical properties and wear mechanism, International Journal of Refractory Metals and Hard Materials 39 (2013) 78-89.

[25] D. Sarkar, M. Kumar B V, B. Basu, Fretting Wear behavior of Ti(CN)-Ni Cermet: Influence of Secondary carbide content; Metals, Materials and Processes 2004; 16:397-402 (2004).

[26] Q. Zhang, S. To, Q. Zhao, B. Guo, Surface damage mechanism of WC/Co and RB-SiC/Si composites under high spindle speed grinding (HSSG), Materials & Design 92 (2016) 378-386.

[27] Q. Zhang, Q. Zhao, S. To, B. Guo, W. Zhai, Diamond wheel wear mechanism and its impact on the surface generation in parallel diamond grinding of RB-SiC/Si, Diamond and Related Materials 74 (2017) 16-23.